A SOLAR DRIVEN THERMOACOUSTIC REFRIGERATOR TACSOL

Maxime Perier-Muzet, Sophie Cordillet, Jean Castaing-Lasvignottes, Patxi Duthil, Maurice - Xavier François, Matthieu Pierens, Thierry Le Pollès, G Olalde, P Stouffs, Jean-Pierre Thermeau, et al.

A SOLAR DRIVEN THERMOACOUSTIC REFRIGERATOR TACSOL

PERIER-MUZET M.[(*)], CORDILLET S.[(**)], CASTAING-LASVIGNOTTES J.[(*)], DUTHIL P.[(***)], FRANÇOIS M.X.[(*****)], PIERENS M.[(***)], LE POLLES T.[(****)], OLALDE G.[(**)], STOUFFS P.[(*)], THERMEAU J.P.[(***)], BEDECARRATS J.P[(*)]

[(*)] Laboratoire de Thermique, Energétique et Procédés, IFR, rue Jules Ferry, Pau, BP 7511 – 64075, France
jean.castaing@univ-pau.fr

[(**)] Laboratoire PROcédés Matriaux et Energie Solaire, 7 rue du Four Solaire, Odeillo, 66120, France

[(***)] Institut de Physique Nucléaire d'Orsay, Orsay, BP1 – 91406, France

[(****)] Hekyom, 2 rue Jean Rostand, Orsay, 91400, France

[(*****)] Hekyom, professor emeritus from the Paris Université Pierre et Marie Curie and LIMSI-CNRS, France

ABSTRACT

Among the alternatives to electrically driven vapour compression cycle for refrigeration, heat driven thermoacoustic refrigerators seem a promising technology. These machines have already proved their capability in laboratory or in space refrigeration. Some previous studies have also demonstrated the possibility of using concentrated solar energy as thermal energy sources for low power heat driven thermoacoustic refrigerators. New investigations are nowadays carried out to improve the efficiency and increase the refrigerating power in order to develop this technology in the industrial refrigeration domain. The aim of the work presented here is to investigate the global performances of a solar driven thermoacoustic refrigerator plant by mean of computer aided modelling. The interest of such refrigerators are introduced in a first part. The modelling, at the system level, of the main elements of the prototype is developed in a second section. Then the first simulation results are presented and analysed.

1. INTRODUCTION

In the current energy and environmental crisis, it becomes important to develop, environmentally friendly, reliable and efficient refrigerators. Among the alternatives, the tri-thermal thermodriven thermoacoustic refrigerator cycle seems to be a promising technology (Zink *et al*., 2010). Compared to the vapor compression cycle which is the most popular technology for cold production, thermoacoustic devices have numerous advantages. They have no moving components, they use nonpolluting working fluids and they can be directly driven by thermal sources like waste heat, fuel gas or solar energy. These machines have already proved their capability in laboratory experiments as well as for specific applications like space refrigeration to reach very low temperatures. New investigations are nowadays carried out to improve the energetic efficiency in order to develop this technology in the industrial refrigeration domain.

Considering that cooling demand increases with the intensity of solar radiation, solar refrigeration has been considered as a logical solution (Kim and Infante Ferreira, 2008). Associated with solar collectors, thermoacoustic systems could be an alternative to the solar sorption and solar thermal refrigeration. Previous studies have already demonstrated the possibility of such an association for low power thermodriven thermoacoustic refrigerators. Chen (2001) describes the construction and the first test measurement of a thermoacoustic cooler powered by a solar parabolic dish collector. Because of working fluid leakages and thermal losses, this cooler achieved only a temperature gap of 1.5°C. Adeff and Hofler (2000) have tested a thermoacoustic refrigerator driven by solar radiation concentrated by Fresnel lens. This refrigerator produced 2.5 W at 5°C with a heat source at 475°C and an ambient temperature at 23°C.

Although the demand for refrigerating power is more important when the sun is shining, the main difficulty of the solar refrigeration is to ensure the demand during the time without sufficient solar radiation. To avoid the impact on the cold supply of the intermittency of the production, energy storage is generally used.

The aim of this work is to present the modeling and the first simulation results of a solar driven thermoacoustic refrigerator plant. The prototype being studied is a heat driven thermoacoustic refrigerator able to deliver a refrigerating power of about 1 kW at -30°C and filled with 40 bar pressurized helium as working fluid. The heat source is obtained by means of concentrated solar energy at a high temperature of about 700°C and supplied by a large parabolic solar concentrator. The time variations of the energy source

impose a particular control of this device. The temperature levels reached by the system while running has lead us to consider a cold storage instead of a hot one due to the more important difficulty to maintain a low level of heat transfer with surroundings at 700°C in comparison to a cold storage at -30°C. Moreover, this device allows a constant power supply whatever the production fluctuations.
The prototype being built and modeled is described firstly in this paper. Secondly the model is presented, taking into account the thermoacoustic refrigerator as well as the cold storage. In the end, results from simulation (temperature levels and ice fraction, exchanged power) are analyzed when considering a few days under sunny conditions.

2. PROTOTYPE DESCRIPTION

The device considered here consists in a solar concentrator, a solar receiver, a thermoacoustic machine composed firstly of a thermoacoustic prime mover linked to an acoustic resonator and secondly of a thermoacoustic refrigerator linked to a cool thermal energy storage (Figure 1).

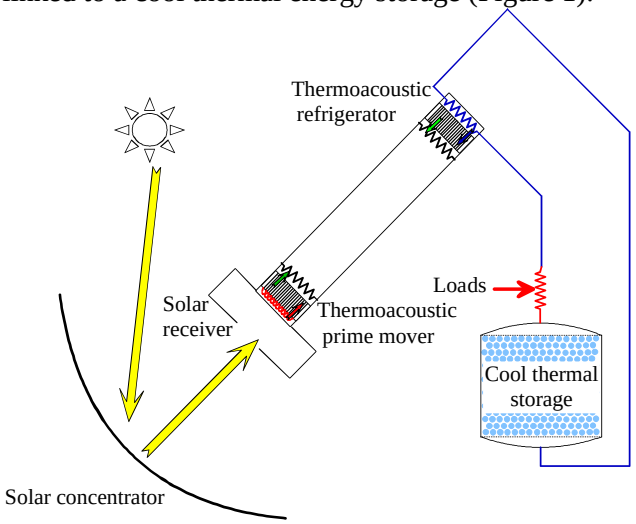

Figure 1. Solar driven thermoacoustic refrigerator experimental plant

The solar driven thermoacoustic refrigerator heat fluxes represented in Figure 2 are described in the following sections. The direct solar radiation is collected, reflected and concentrated by a parabolic mirror. More details on this element can be found in Nepveu *et al*. (2009). The surface collector is adjusted in order to reflect a power of approximately 6.8 kW. Concentrated solar radiation is collected by an absorber situated in a receiver cavity. This latter transfers approximately 4.4 kW to the working fluid (helium at about 40 bar), while being at a temperature close to 700°C. More details on this component can be found in Cordillet *et al.* (2010).

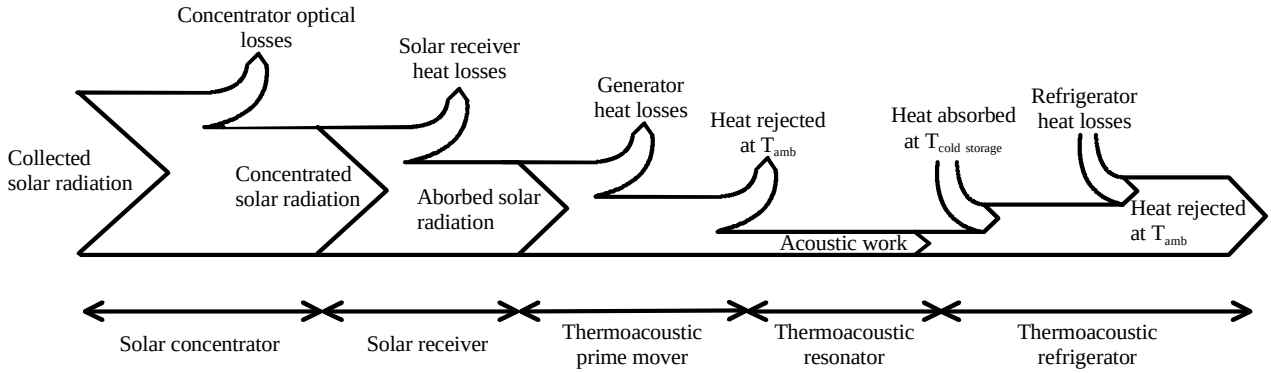

Figure 2. Solar driven thermoacoustic refrigerator heat fluxes

The thermoacoustic cooler is composed of a wave generator, an acoustic resonator and a thermoacoustic refrigerator. Thank to the solar energy, the thermoacoustic prime mover generates a traveling wave with a large acoustic power. This latter is used into the thermoacoustic refrigerator to pump approximately 1 kW of

heat from the cold heat exchanger and reject it at the intermediate temperature exchanger of the refrigerator. A detailed explanation of the way these coolers work is given by Swift (2002).
To ensure a constant power at the cold exchanger, a latent storage is intended to be used. This later uses encapsulated nodules filled with an eutectic Phase Change Material (PCM). The storage tank is filled with these nodules and the cold transfer fluid which circulated in the tank ensures the heat exchange between the PCM and the cold production unit. When the tank is being cooled, the crystallization of nodules allows the storage of the energy. For more details refer to Bedecarrats and Dumas (1997).
To produce a controlled thermal load, an electrical fluid circulation heater is placed between the storage tank and the cold heat exchanger. The power regulation of this latter allows generating different load profiles and storage strategies.

3. MODELING

To help designing the prototype and to determine its future energetic performances, a lumped model of the entire plant has been developed. The time variation of the energy source and of refrigeration loads imposes a transient approach. All components of the machine are treated by transient models while a quasi-stationary approach it used for the thermodriven thermoacoustic refrigerator.

3.1. The solar driven thermoacoustic refrigerator

A uniform wall temperature for each heat exchangers of the thermoacoustic device have been considered in the model.

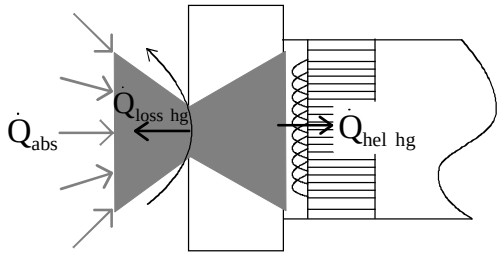

Figure 3. Scheme of the hot exchanger of the thermoacoustic generator

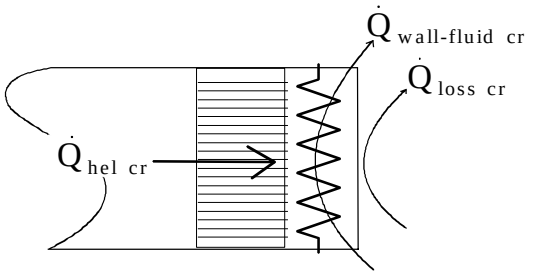

Figure 4. Scheme of the cold exchanger of the thermoacoustic refrigerator

The hot exchanger of the thermoacoustic generator absorbs the solar radiation reflected by the concentrator and transfers the major part of this heat flux to the working fluid (Figure 3), the rest being exchanged with surroundings. The energy balance of this element can be written as:

$$\frac{dU_{hg}}{dt} = \dot{Q}_{abs} + \dot{Q}_{loss\ hg} + \dot{Q}_{hel-wall\ hg} \tag{1}$$

The solar power absorbed is calculate by $\dot{Q}_{abs} = DNI.\rho.S_{abs}.\chi$, where DNI is the Direct Normal Irradiation, ρ the reflectivity, χ the concentration factor and S_{abs} the area of the absorber. The heat losses from the solar absorber cavity wall are neglected face to the radiative and convective losses through its orifice. These losses are determined by $\dot{Q}_{loss\ hg} = S_{or}\left[\alpha_{or}.\left(T_{amb} - T_{hg}\right) + \varepsilon_{or}.\sigma.\left(T_{amb}^{\ 4} - T_{hg}^{\ 4}\right)\right]$ where the convective heat exchange coefficient between the orifice and the surrounding (α_{or}) is estimated from Nepveu (2008).

The cold exchanger of the refrigerator (Figure 4) as well as the heat exchangers at intermediate temperature transfer on one side with the helium and on the other with a heat transfer fluid. The cold one is submitted to heat transfer with surroundings while such an exchange is neglected for the other ones because of the low temperature difference between these exchangers and ambient air. Applying first law to the wall and to the heat transfer fluid of these elements gives:

$$\begin{cases} \dfrac{dU_{wall\ exchanger}}{dt} = \dot{Q}_{fluid-wall\ exchanger} + \dot{Q}_{hel-wall\ exchanger} + \dot{Q}_{loss\ exchanger} \\ \dfrac{dU_{fluid\ exchanger}}{dt} = \dot{Q}_{wall-fluid\ exchanger} + \dot{m}_{fluid\ exchanger}\left(h_{fluid\ in\ exchanger} - h_{fluid\ out\ exchanger}\right) \end{cases} \tag{2}$$

The convective heat transfers between the heat exchanger walls and the fluids are given by $\dot{Q}_{fluid-wall} = \alpha_{fluid-wall}.S_{fluid-wall}.\Delta TML_{fluid-wall}$ where the heat exchange coefficients ($\alpha_{fluid\ wall}$) are calculate thanks to a correlation for a fluid flowing across a bank of tubes proposed by Zukauskas (1987).
Each equation relative to the exchanger walls has a term of transfer with helium. A stationary model, whose details are described in François and Bretagne, is used to determine these heat fluxes at each time step of the quasi-stationary model (Perier *et al*, 2010).

3.2. The cool thermal energy storage

The simplified model of the cool thermal energy storage proposed for this study is based on the one developed by Bédécarrats *et al*. (2009).

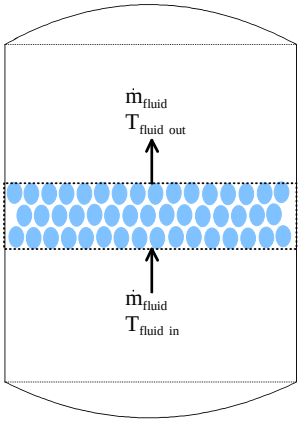

Figure 5. Tank control volume

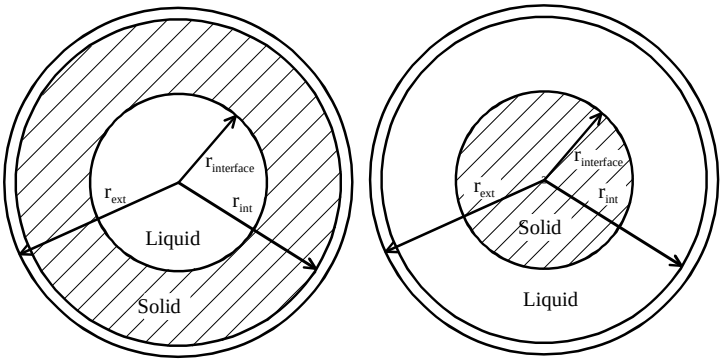

Figure 6. Crystallization inside nodule at left and melting inside the nodule at right

We considered a perfectly insulated vertical tank filled with PCM nodules. The heat transfer fluid circulates from the bottom to the top of the tank for both charge and discharge mode. The flow in the tank is assumed incompressible and the variation of temperature of the heat transfer fluid is only along the axial direction. Thermal conduction is neglected in the heat transfer fluid as well as between the nodules themselves. The tank is divided in 5 control volumes according to the height (Figure 5) and we assumed that the nodules of the same control volume have exactly the same behaviour (temperature, solid fraction …) and that they are not submitted to any volume variation. Crystallization and melting are supposed beginning on the inner surface of the envelope and that the solid or respectively the liquid zone grows concentrically towards the centre (Figure 6). We assume that in case of charge after a partially discharge of the nodule, the remaining crystal is attached on the envelope of the nodule and grows concentrically to the center. Supercooling effect has not being taken into account in the model. When the nodule is totally crystallized or totally melted, the temperature is supposed uniform in the nodule. Due to expansion of the PCM volume during the crystallization, the nodules are not completely filled with PCM and a very small volume is left empty in each of them to absorb the volume increase.
The variation of the internal energy of the fluid for each tank control volume (Figure 4) can be written:

$$\frac{dU_{fluid}}{dt} = \dot{m}_{fluid}\left(h_{fluid\ in} - h_{fluid\ out}\right) + N_{nod}\,\dot{Q}_{fluid-nod} \tag{3}$$

Applying first law to a nodule gives:

$$\frac{dU_{nod}}{dt} = m_{nod}\frac{du_{nod}}{dt} = \dot{Q}_{nod-fluid} \tag{4}$$

With:

$$u_{nod} = \begin{cases} u_{ref} + Cv_{PCM\ solid}\left(T_{nod} - T_{ref}\right) & \text{if} \quad T_{nod} < T_{melt} \\ u_{ref} + Cv_{PCM\ solid}\left(T_{melt} - T_{ref}\right) + x_{solid}\ L & \text{if} \quad T_{nod} = T_{melt} \\ u_{ref} + Cv_{PCM\ solid}\left(T_{melt} - T_{ref}\right) + L + Cv_{PCM\ liq}\left(T_{nod} - T_{ref}\right) & \text{if} \quad T_{nod} > T_{melt} \end{cases} \tag{5}$$

The heat exchange between the heat transfer fluid and a nodule is expressed by $\dot{Q}_{fluid-nod} = \frac{T_{nod} - T_{fluid}}{R_{ext} + R_{env} + R_{int}}$ where R_{ext}, R_{env}, R_{int} are respectively the external, the envelope and the internal nodule thermal resistances. They are given by $R_{ext} = \frac{1}{4\pi r_{ext}^2 \alpha_{ext}}$ with $\alpha_{ext} = \frac{k_{fluid}}{2 r_{ext}} Pr^{1/3} Re^{1/2}$ and $R_{env} = \frac{1}{4\pi k_{env}} \left(\frac{1}{r_{int}} - \frac{1}{r_{ext}} \right)$

Concerning the internal nodule thermal resistance, three different cases have to be considered:

- the nodule is totally meted or crystallized: $R_{int} = 0$
- the nodule is under crystallization: $R_{int} = \frac{1}{4\pi k_{PCM\ solid}} \left(\frac{1}{r_{interface}} - \frac{1}{r_{int}} \right)$
- the nodule is under melting: $R_{int} = \frac{1}{4\pi k_{PCM\ liq\ eq}} \left(\frac{1}{r_{interface}} - \frac{1}{r_{int}} \right)$

In this last case, natural convection in the liquid phase is taken into account using an equivalent thermal conductivity of the liquid phase ($k_{PCM\ liq\ eq}$), experimentally determined by Bédécarrats *et al*. (2009).
The radius of the interface ($r_{interface}$) is calculated in both charge or discharge mode by means of the solid fraction (x_{solid}) determined in eq. 5.

4. FIRST RESULTS

The main parameters that have been used for simulation are summarized in the table 1. To be independent of initial conditions, four same days have been applied to the model in terms of DNI (figure 7).

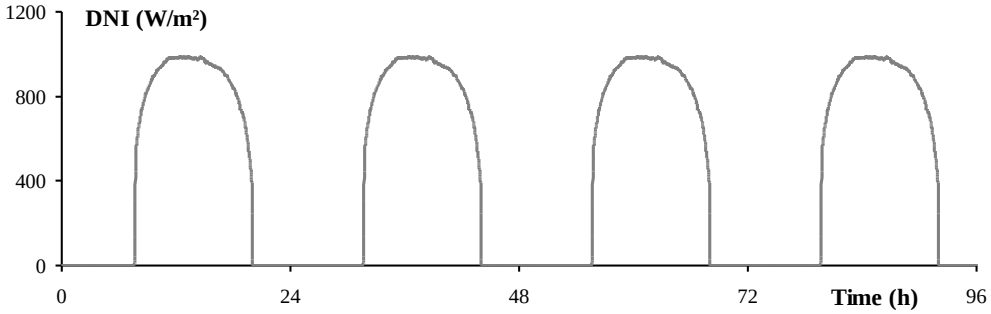

Figure 7: DNI applied to the simulated thermoacoustic refrigerator.

Table 1. Main parameters of the model.

Concentration factor χ (-)	700	Absorber area (m^2)	4e-3
Reflectivity ρ (-)	0.925	Orifice area (m^2)	1.8e-2
Cold and intermediate heat exchanger mass (kg)	1	Hot heat exchanger mass (kg)	10
Melting temperature T_{melt} (°C)	21.1	Tank volume (m^3)	0.2

The consequence of this solar heat flow is shown in figure 8 where the temperature of the hot heat exchanger wall is represented. Due to a very low inertia of the heat exchanger, the temperature evolutions are quite rapid when the sun is shining. On the contrary and due only to thermal losses, the heat exchanger is slowly cooled down at night. When heated, the machine starts (pressure and mass flow wave inside the tube) only if a sufficient temperature difference exists between the two heat exchangers of the engine cycle. As the environment temperature is quite constant and close to 20 °C and according to previous experimentations, a temperature of 600 K as been set as the minimum one for the cycle to operate. On the contrary, the machine stops when the hot heat exchanger temperature gets lower than this value.

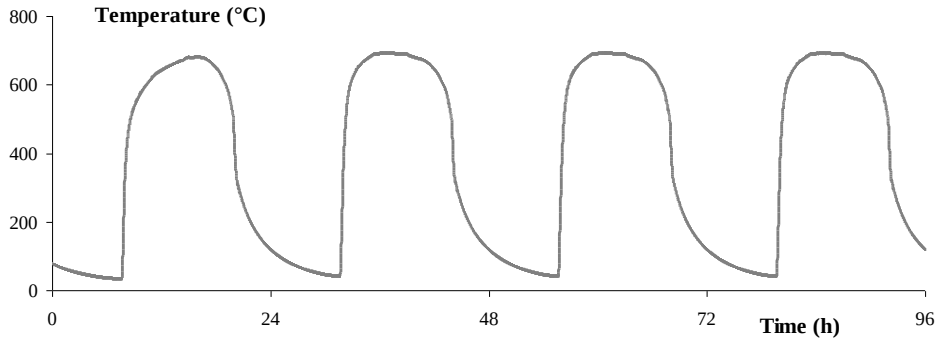

Figure 8: Generator hot heat exchanger temperature

To cool down the intermediate heat exchangers, a flow rate of water at 20°C is used. Output temperatures are represented in figure 9. Due to their high efficiencies (shell and tubes heat exchanger with 1.6 mm inner copper tubes), these heat exchangers remain quite close to this sink temperature.

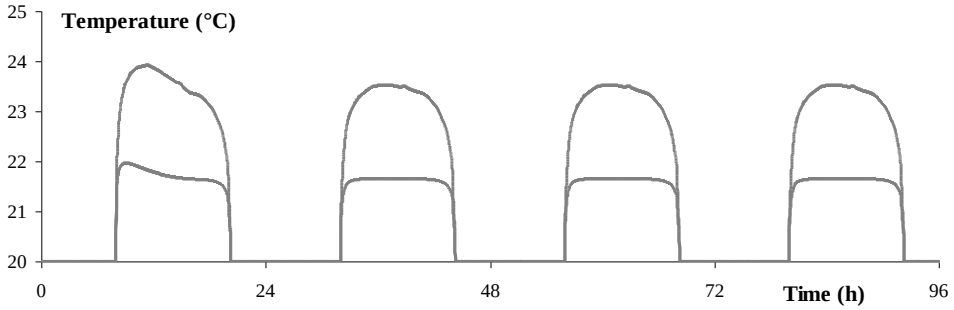

Figure 9: intermediate heat exchanger temperatures

To charge correctly the cold storage, thermal loads are applied to the system only when the cold thermal storage is partially crystallized and a delay of 30 h after the startup has been set (figures 10 and 11).

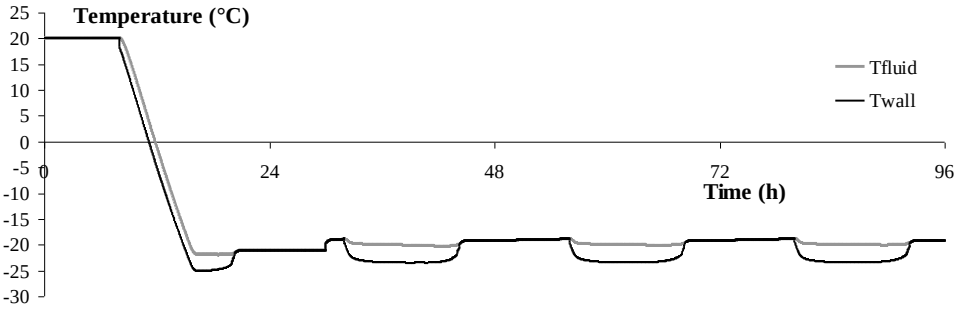

Figure 10: Refrigerator cold heat exchanger temperatures

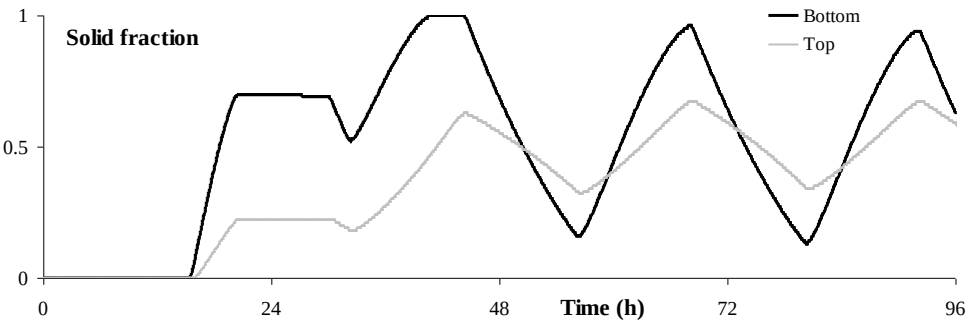

Figure 11: Solid fraction at the top and the bottom of the tank.

Looking at figure 11 allows concluding that the machine reaches periodically steady states conditions after 3/4 days, when the storage tank solid fraction evolves between same levels from one day to the other. It has to be noted also that the heat transfer fluid flowing from the bottom to the top of the tank, the heterogeneity is quite important regarding solid fraction. Due to exchanged latent heat, these important evolutions have light consequences on the low temperature level reached by the cold heat exchanger (figure 10).

5. DISCUSSION AND CONCLUSIONS

The first results obtain from the presented work are encouraging since the prototype that will be built soon and tested next summer has been designed quite correctly. Nevertheless, the simulated results concern only nominal conditions i.e. when solar radiation is of high quality (high level of DNI and unclouded sky). Work is being made at the moment to analyse simulation results when not so ideal conditions are applied to the cycle. This will in particular allow optimizing for instance the size of the tank to face these variations over time. When built, the results from the prototype will then be compared to the model to eventually complete that latter and/or validate it.

6. ACKNOWLEDGEMENTS

This study is funded by the ANR TACSOL (PRECODD 2008).

7. SYMBOL NOMENCLATURE

C	specific heat, J kg^{-1} K^{-1}
χ	concentration factor
DNI	Direct Normal Irradiation, W m^{-2}
DTML	logarithmic difference of temperature, K
H	enthalpy, J kg^{-1}
K	thermal conductivity W m^{-1} K^{-1}
L	Latent heat of the PCM, J kg^{-1}
M	mass, kg
$\dot{m}$	mass flow rate, $kg.s^{-1}$
N	number of nodules in the tank layer
Pr	Prandtl number
$\dot{Q}$	power, W
R	radius, m
R	thermal resistance, K m^{-2} W^{-1}
Re	Reynolds number
S	surface, m^2
T	time, s
T	temperature, K
U	specific internal energy, J/kg
U	internal energy, J
x_{solid}	solid fraction of PCM

Greek symbols:

α	heat transfer coefficient, W m^{-2} K^{-1}
ε	Emissivity
ρ	Reflectivity
σ	Stefan–Boltzmann constant, W m^{-2} K^{-4}

Subscripts

abs	absorbed
amb	ambient
env	nodules envelope
exchanger	heat exchanger
ext	external
fluid	heat transfer fluid
hel	helium
hg	hot exchanger of the generator
in	Inlet
int	internal
interface	interface liquid/solid of the PCM
liq	liquid phase of the PCM
loss	thermal losses
melt	melting of the PCM
nod	nodule
or	orifice of the solar receiver
out	putlet
PCM	Phase Change Material
ref	reference
solid	solid phase of the PCM
wall	wall of the heat exchangers

8. REFERENCES

Zink F., Vipperman J. S., Schaefer L. A. 2010, Environmental motivation to switch to thermoacoustic refrigeration, *Applied Thermal Engineering* 30: 119–126.

Kim D.S., Infante Ferreira C.A. 2008, Solar refrigeration options – a state-of-the-art review, *Int. J. Refrigeration* 31, 3-15.

Chen R.L. 2001, *Design, Construction, and Measurement of a Larger Solar Powered Thermoacoustic Cooler*, Pennsylvania State University.

Adeff J. A., Hofler T. J. 2000, Design and construction of a solar-powered, thermoacoustically driven, thermoacoustic refrigerator, *in: Acoustical Society of America 139th Meeting Press Release*, Melville, New York.

Nepveu F., Ferriere A., Bataille F. 2009, Thermal model of a dish/Stirling systems, *Solar Energy*: 83: 81–89.

Cordillet S., Duthil P., Nepveu F., Le Pollès T., Olalde G., Salome A., Thermeau J-P. 2010, Theoretical proof of concept of an optimal solar receiver to produce low-temperature (-40°C) cooling using a thermoacoustic tri-thermal machine, *Proc. 17th Solar PACES International Symposium*, Perpignan, France.

Swift G.W. 2002, *Thermoacoustics: A Unifying Perspective for Some Engines and Refrigerators*, Acoustical Society of America Publication.

Bédécarrats J.P, Dumas J.P 1997, Etude de la cristallisation de nodules contenant un matériau à changement de phase en vue du stockage par chaleur latente, *Int. J. Heat Mass Transfer* 40(1):149-157.

Nepveu F. 2008, *Production décentralisée d'électricité et de chaleur par système Parabole/Stirling : Application au système EURODISH*, Thèse de Doctorat, Université de Perpignan.

Zukauskas A. 1987 "Heat Transfer from Tubes in Cross Flow." In *Handbook of Single Phase Convective Heat Transfer*, Eds. S. Kakac, R. K. Shah, and Win Aung. New York: Wiley Interscience.

François M.X., Bretagne E., « Echangeurs de chaleur pour application aux fluides oscillants et notamment dans une cellule thermoacoustique. » Brevet PCT/FR03/03591.

Bédécarrats J.P, Castaing-Lasvignottes J., Strub F., Dumas J.P 2009, Study of a phase change energy storage using spherical capsules. Part II: Numerical modeling, *Energy Conversion and Management* 50: 2537-2546.